Nanoscale

Scalable Nanomanufacturing of Holey Graphene via Chemical Etching: An Investigation on Process Mechanisms

Journal:	*Nanoscale*
Manuscript ID	NR-ART-12-2021-008437.R1
Article Type:	Paper
Date Submitted by the Author:	06-Feb-2022

Complete List of Authors:	Bi, Kun; Arizona State University, Materials Science and Engineering Wang, Dini; Arizona State University, Materials Science and Engineering Dai, Rui; Arizona State University, Mechanical Engineering Liu, Lei; Arizona State University Wang, Yan; University of Nevada Reno, Mechanical Engineering Lu, Yong-Feng; University of Nebraska-Lincoln, Electrical & Computer Engineering Liao, Yiliang; Iowa State University, Industrial & Manufacturing Systems Engineering Ding, Ling; Wuhan University of Science and Technology, School of Chemistry and Chemical Engineering Zhuang, Houlong; Arizona State University, Mechanical Engineering Nian, Qiong; Arizona State University, Mechanical Engineering

ARTICLE

Scalable Nanomanufacturing of Holey Graphene via Chemical Etching: An Investigation on Process Mechanisms

Received 00th January 20xx,
Accepted 00th January 20xx

DOI: 10.1039/x0xx00000x

Kun Bi, [#a] Dini Wang, [#a] Rui Dai, [#a], Lei Liu, [a] Yan Wang, [b] Yongfeng Lu, [c] Yiliang Liao, [d] Ling Ding, [e] Houlong Zhuang, [a] and Qiong Nian *[a]

Graphene with in-plane nanoholes, named holey graphene, shows great potential in electrochemical applications due to the fast mass transport and the improved electrochemical activity. Scalable nanomanufacturing of holey graphene is generally based on chemical etching using hydrogen peroxide to form through-the-thickness nanoholes on the basal plane of graphene. In this study, we probe into the fundamental mechanisms of nanohole formation under peroxide etching via an integrated experimental and computational effort. The research results show that the growth of nanoholes during etching of graphene oxide is achieved by a three-stage reduction-oxidation-reduction procedure. First, it is demonstrated that vacancy defects are formed via a partial reduction-based pretreatment. Second, the hydrogen peroxide reacts preferentially with the edge-sites of defect areas on graphene oxide sheets, leading to the formation of various oxygen-containing functional groups. Third, the carbon atoms around the defects are removed along with the neighboring carbon atoms via reduction. By advancing the understanding of process mechanisms, we further demonstrate an improved nanomanufacturing strategy, in which graphene oxide with a high density of defects is introduced for peroxide etching, leading to the enhanced nanohole formation.

1 Introduction

Graphene with in-plane nanoholes, also known as holey graphene, has been extensively studied in recent years to improve the performance of graphene-based electrochemical devices. The improved performance is attributed to the abundant mass transport channels provided by the nanoholes and the chemically active edge-carbon atoms surrounding the nanoholes.[1] These new features brought by the in-plane nanoholes can overcome the most inevitable issues, including re-stacking and lacking of electrochemical activity,[2] of pristine graphene. As a result, the active specific surface area of graphene can be drastically increased, despite that electrical conductivity is slightly scarified. For instance, Y. Bai *et al*.[3] reported that the electrical conductivity decreased from 3287 to 1786 S m^{-1} after the formation of nanoholes on graphene sheets. However, the volumetric capacitance and rate capability of the thin-film electrodes were largely increased due to the improved ion diffusion kinetics. Similar results can be found in the research on holey graphene-based supercapacitors[4] or lithium-ion batteries[5]. To date, an increasing number of studies have demonstrated the superior performance of holey graphene in specific surface area[6], specific capacitance[7], and charge transfer rate[8], which are the most significant factors affecting the performance of various electrochemical applications.

To fabricate holey graphene, the most prevalent nanomanufacturing method is to etch graphene oxide (GO) with oxidative chemicals, such as hydrogen peroxide (H_2O_2)[6], nitric acid[9], and oxygen[10]. Among those etchants, H_2O_2 has been widely used due to the following advantages. First, it is a green process without any highly aggressive etchant and toxic by-product. Second, it is a solution-based process, which allows thorough mixing of GO sheets and H_2O_2 molecules, avoiding non-uniform chemical reactions and facilitating the control of the reactions. The solution product can be directly stored or readily used for further processing, such as hydrothermal synthesis and freeze-drying to obtain free-standing, hierarchical porous structures of holey graphene[11]. Third, it is suitable for the electrochemical applications since it does not require high-cost equipment or strict environment, which are often seen in the bottom-up methods for fabrication of semiconductor-level holey graphene sheets[12].

Although nanomanufacturing of holey graphene using H_2O_2 etching has been established experimentally, the process mechanism in terms of the formation of nanoholes remains elusive. Previous studies generally agreed that the etching reactions can be attributed to the chemical oxidation by the etchant. The chemical oxidation breaks the covalent carbon-

[a.] *School of Engineering for Matter, Transport and Energy, Arizona State University, Tempe, AZ, 85287, USA*
[b.] *Department of Mechanical Engineering, University of Nevada, Reno, NV 89557, USA*
[c.] *Department of Electrical & Computer Engineering, University of Nebraska-Lincoln, Lincoln, NE 68588, USA*
[d.] *Department of Industrial & Manufacturing Systems Engineering, Iowa State University, Ames, IA 50011, USA*
[e.] *School of Chemistry and Chemical Engineering, Wuhan University of Science and Technology, Wuhan 430081, People's Republic of China*
# All authors contributed equally
* Corresponding author: Qiong.Nian@asu.edu

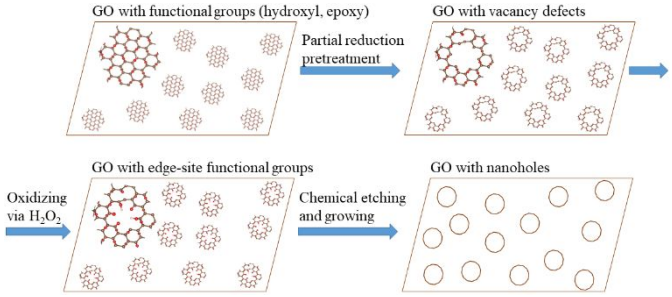

carbon bonds, leads to the formation of carboxylic compounds, and results in carbon atom removal as well as the nucleation

Fig. 1 Schematic diagram of the vacancy defect generation and growth into nanoholes on GO sheets.

and growth of in-plane holes. Due to the high bonding energy of the π-π conjugation, a long processing time and extreme etching conditions were often utilized. However, J.G. Radich *et al.* pointed out that the etching reactions could be significantly promoted by pre-existing vacancy defects and local kinetics[13]. They tested the hypothesis by a partial reduction process to generate vacancies and then applied UV irradiation to promote the etching reactions. Although these studies are encouraging, several essential aspects of the formation mechanism of nanoholes on graphene basal planes remain unclear, e.g., how the partial reduction pretreatment generates vacancies, how the atomic vacancies facilitate the etching reactions, and what are the reaction mechanisms between H_2O_2 and the graphene basal planes with/without pre-existing vacancies. Prior studies claimed that H_2O_2 tends to activate into hydroxyl radicals to react with the graphene sheets and eventually result in in-plane hole formation[14]. Other researchers incline to believe that the hole formation is mainly caused by the oxidizing property of H_2O_2[15] itself. However, no experimental nor simulation results have been reported to support these assumptions.

In this study, the fundamental mechanism of nanohole formation in holey graphene under peroxide etching is investigated via an integrated experimental and computational effort. We first demonstrate the formation mechanisms of vacancy defects on GO sheets under partial reduction-based pretreatments using molecular dynamics (MD) simulations. Then, the reactions and products between H_2O_2 and various forms of graphene (e.g., with and without vacancy defects) are investigated by density functional theory (DFT) calculations. Afterwards, the mechanism for the continuous growth of atomic vacancies into in-plane nanoholes under H_2O_2 etching is revealed by MD simulations and verified by experiments. Basing on our study, we come up with a schematic diagram in Figure 1 to illustrate how vacancies are generated and then grow into nanoholes under peroxide etching, which will be discussed in three steps in following sections.

2 Results and discussion

First of all, how vacancy defects are formed by a partial reduction-based pretreatment of GO is investigated. It is well known that thermal annealing is a common method for reducing GO, which removes not only the functional groups but also the in-plane carbon atoms to form vacancy defects.[16] Oxygen-containing functional groups, such as the hydroxyl and epoxy groups, weaken the π–π conjugations and increase the activity of neighboring carbon atoms. During annealing, the hydroxyl and epoxy groups remove carbon atoms from the graphitic lattice to form the gaseous species that eventually leave the system. Therefore, thermal annealing, if used as the partial reduction pretreatment, could generate in-plane vacancy defects on graphene sheets. Herein, MD simulations were carried out to study the carbon-atom removal mechanism during thermal annealing of GO sheets. In the simulation, a constant temperature increase rate of 8 K fs^{-1} was applied on a GO model until it reached a target temperature, and the temperature was held unchanged to the end. The gaseous products, such as CO, CO_2, and H_2O, were removed from the simulation box immediately after generation during the whole process.

The initial structure of the GO model (Figure 2a) is a graphene sheet randomly anchored by the functional groups that commonly found in experiments (i.e., the hydroxyl and epoxy groups)[16, 17]. After annealing at 1000 K (Figure 2b), no carbon atom is removed from GO throughout the whole simulation (Figure 2h), but a few six-atom graphitic rings with rich functional groups are teared off due to the breakage of the sp^2 C–C conjugation, resulting in the emergence of the small in-plane vacancy defects in these locations. By increasing the target temperature to 1500 K (Figure 2c), the breakage of graphitic rings is more evident. The removal of carbon atoms (1%) is observed under this temperature (Figure 2h). Temperatures of 2000 and 2500 K (Figure 2d and 2e) only cause slightly higher atom loss percentages (ca. 2%), but the sizes of in-plane vacancy defects become larger. The formation of these vacancy defects is attributed to not only the reduction reaction of functional groups, but also the physical damage of the graphene lattice by the high kinetic energy input into the model. This can be further verified by the annealing at 3000 and 3500 K (Figures 2f and 2g), which exhibits severe graphene lattice degradation. The breakage of graphitic rings is not limited to the locations rich of functional groups but extends to the whole lattice. The atom loss percentage surges to ca. 8% at 3000 K and 18% at 3500 K, respectively. Figure 2h shows that the carbon atom loss percentages at different temperatures all stabilize after certain time, indicating no further reduction reaction to occur once the functional groups are consumed. The continuous energy input does not bring about continuous carbon atom removal and the breakage of graphitic rings, indicating that the formation of the in-plane vacancies and lattice defects during thermal reduction is determined by the annealing temperature. A high reduction annealing temperature can easily lead to severe lattice degradation. It should be noted that this rule is tenable when the number of the pre-occupied oxygen-containing groups is a constant. In summary, the MD simulation results suggest that, although it can cause the formation of in-plane vacancies, the reduction-based pretreatment cannot sustain a continuous growth of large nanoholes without inducing severe degradation of the neighboring graphitic rings. This is attributed to the stop of carbon atom removal once

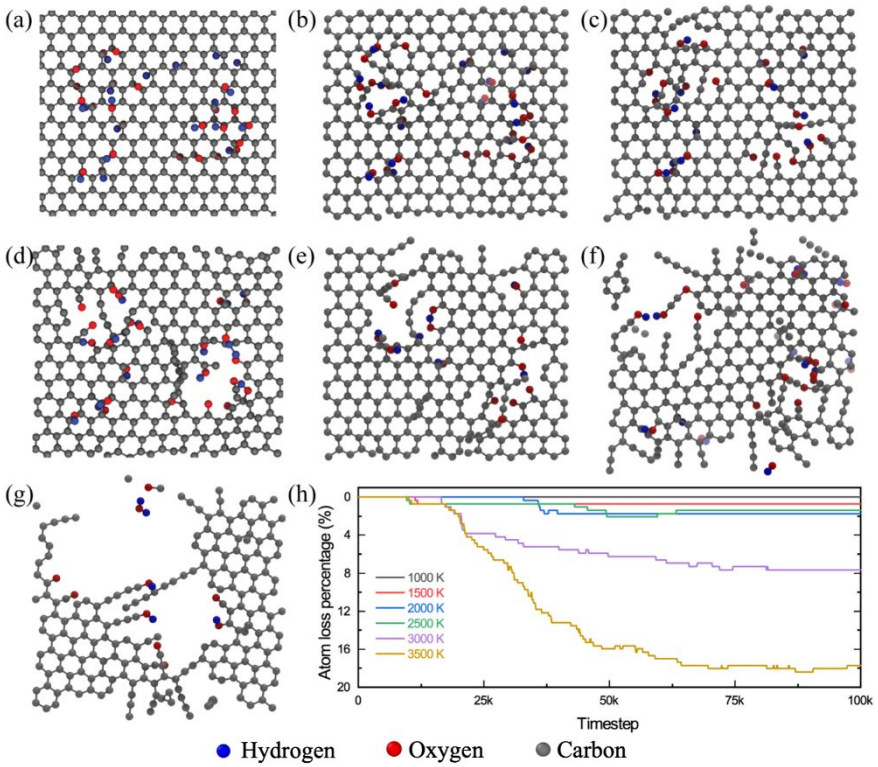

Fig. 2 MD simulations of the thermal annealing process of GO at various temperatures: (a) the initial model; (b–g) the models after annealing at 1000, 1500, 2000, 2500, 3000, and 3500 K; (h) sp2 carbon atom loss percentage of the graphene model with respect to the time step of the simulation.

reactive functional groups are fully consumed during the thermal reduction process.

Simulation results in Figure 2 demonstrate the effectiveness and limitation of the partial reduction-based pretreatment process (i.e., thermal annealing) on the formation of vacancy defects. This indicates further oxidation reaction is needed to restore reactive functional groups to the atomic sites surrounding vacancy defects, if continuous removal of carbon atoms and thereby the growth of nanoholes are needed.

Herein, it is hypothesized that the H_2O_2-graphene reaction can add functional groups to the edge sites of vacancy defects. To understand how the H_2O_2 etchant reacts with graphene, and the impact of pretreatment generated vacancy defects on the oxidation reaction kinetics, DFT calculations were conducted. According to prior experimental studies[15, 18], there are two plausible ways of how graphene is oxidized by H_2O_2: A) H_2O_2 molecules directly react with graphene; and B) H_2O_2 molecules are first energized to form the hydroxyl radicals (·OH), which then react with graphene. In the calculation for the situation A, a H_2O_2 molecule was placed at the centers of four graphene models, the results were shown in our previous publication[19]; for the situation B, a hydroxyl radical was placed on the same locations, the results are shown in Figure 3.

The effects of the pre-existing functional groups and pretreatment vacancy defects on the H_2O_2 oxidation reactions were revealed by four graphene models, i.e., pristine graphene (Figure 3a), GO (one epoxy group in each unit cell of the graphitic ring, Figure 3b), graphene with a vacancy defect (a six-atom ring is taken away from the graphene lattice, Figure 3c), and GO with a vacancy defect (Figure 3d). Each of the calculations ends until the global minimum of the system energy is achieved. The energy change from the initial to the end of the calculation can indicate the possibility of each reaction to take place according to the Boltzmann statistics.

The DFT results in Figure 3 indicate that the reactions only take place in the cases of graphene and GO with a vacancy defect (Figures 3c and 3d), in which the corresponding energy changes are −8.30 and −9.37 eV (Table 1), respectively. Interestingly, in both cases, the edge-site carbon atoms around the vacancy defect are the preferred targets attacked by the hydroxyl radicals. For the graphene model with a vacancy defect (Figure 3c), the edge-site carbon atoms are anchored by a carbonyl and a hydrogen group. Besides, a hydroxyl group can be anchored onto the graphene basal plane (Figure 3a), although the energy change is much lower without a pretreatment vacancy defect. For the GO model with a vacancy defect (Figure 3d), one edge-site carbon atom is anchored by a carbonyl group. This agrees well with prior experimental studies demonstrating that the edge carbon atoms are more chemically active comparing to basal-plane carbon atoms[20]. In addition, as shown in Table 1 that the reactions between these edge-carbon atoms and hydroxyl radicals are more thermodynamically favorable due to a larger energy change than the reactions with H_2O_2 molecules (i.e., −7.06 and −7.03 eV energy change[19]). The calculation results suggest that the H_2O_2 oxidation reaction can be promoted if the H_2O_2 radicalization process can be catalyzed,

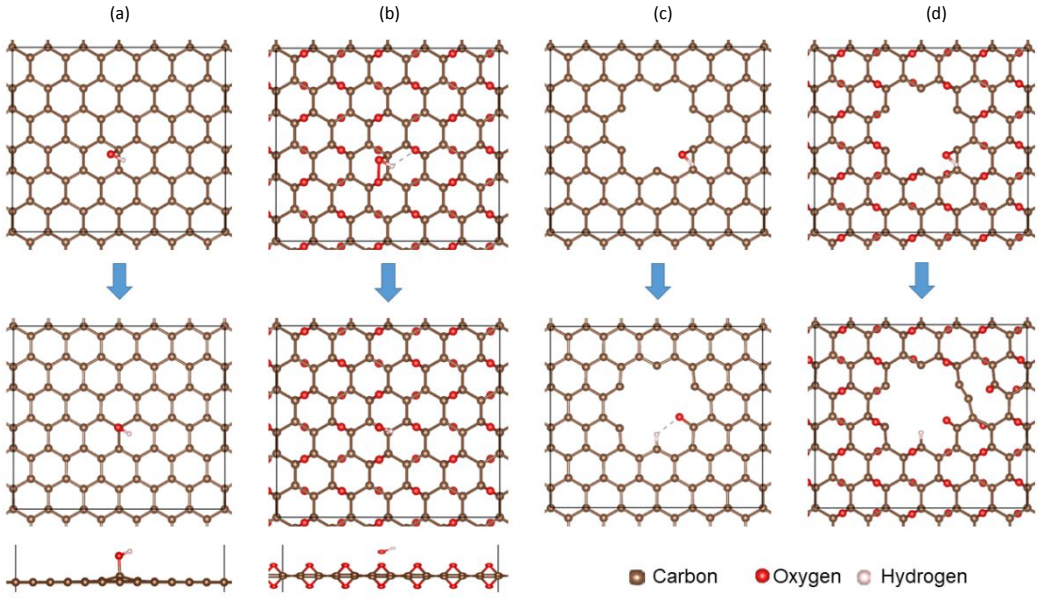

Fig. 3 Models for DFT calculations of the reactions between a hydroxyl radical and (a) graphene, (b) graphene oxide, (c) graphene with a vacancy defect, and (d) graphene oxide with a vacancy defect, respectively.

Table 1 Products and energy changes of the reactions between graphene and hydrogen peroxide or hydroxyl radicals.

Initial material	Products with H_2O_2	Products with ·OH	ΔE with H_2O_2	ΔE with ·OH
Graphene	\	C–OH	-0.08 eV	-2.06 eV
GO	\	\	-0.12 eV	-0.09 eV
Graphene w/ a vacancy	C=O, C–H, C–OH	C=O, C–H	-7.06 eV	-8.30 eV
GO w/ a vacancy	C=O, H_2O	C=O, C–H	-7.03 eV	-9.37eV

which well explains the prior experiment results by J.G. Radich *et al*. However, without metal or other similar catalysts that are often required to activate the H_2O_2 radicalization, the oxidation reactions are mainly attributed to H_2O_2 molecules themselves. The products of the H_2O_2 molecules reacting with the edge-carbon atoms are shown in Table 1 as well, including carbonyl, hydroxyl, and hydrogen groups.

For all reactions aforementioned, the results are the adsorption of oxygen-containing groups to the carbon atoms without a direct carbon atom removal, indicating that H_2O_2 can only oxidize the graphene sheets instead of directly taking away carbon atoms. In an actual reaction, a GO sheet may contain the features in local areas similar to those four different graphene models. The areas with vacancy defects are more vulnerable than the intact areas on the GO sheet. The H_2O_2 molecules prefer to oxidize the carbon atoms surrounding the vacancy defects, forming mainly carbonyl, hydroxyl, and hydrogen groups. When these newly restored functional groups go through reduction process again as demonstrated in Figure 2, the edge-carbon atoms will be removed and vacancy defects (or small size atomic holes) on the GO sheets can grow into larger size nanoholes without inducing severe lattice degradation. In addition, the vacancy-to-nanohole growth process is generally controllable, as it stops once the added functional groups are consumed or kinetical energy input for reduction process is suspended. To sum up our computation study shown in Figures 2 and 3, we consider the partial reduction pretreatment process forms vacancy defects to initiate the hole formation, then H_2O_2 oxidation restores reactive functional groups and following repeat reduction process enables the hole growth, as shown in Figure 1. In practical experiments, these reduction-oxidation-reduction reactions happen continuously so that large nanoholes are formed in multiple locations on a graphene basal plane. This process will be studied next and experimentally verified thereafter.

To confirm whether H_2O_2 oxidation and the following repeat reduction processes can induce the continuous growth of atomic vacancies into large-size nanoholes, MD simulation of GO under thermal annealing at 1000 K in Figure 2 is adapted again but coupled with the chemical reactions between H_2O_2 and GO. In specific, after each time the GO model stabilizes under annealing-based reduction, additional hydroxyl and carbonyl groups are manually added back to the carbon atoms to mimic the oxidation by H_2O_2, which will be followed by another run of thermal annealing-based reduction process. During the entire simulation, the oxidation and annealing are alternatingly repeated two and three times. Note that, as demonstrated by the DFT calculations, the edge-site carbon atoms surrounding the vacancy defects are chemically active and prone to be oxidized by H_2O_2. Therefore, the oxygen-containing functional groups are manually anchored onto those locations, which are assumed to weaken the bonding strength of these carbon atoms.

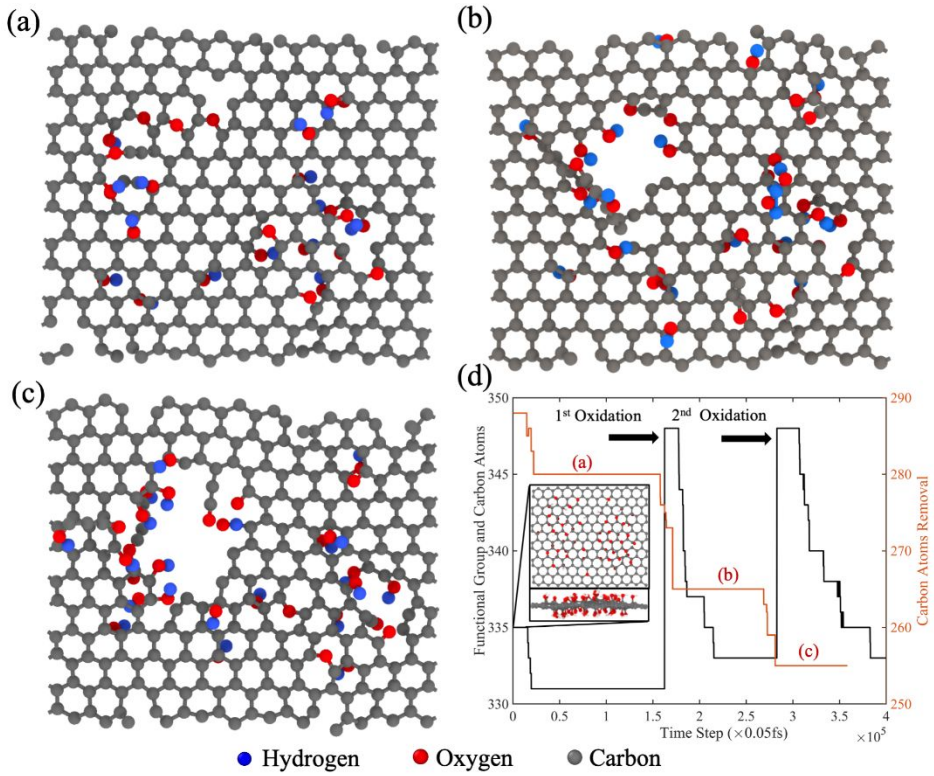

Fig. 4 MD simulations of the vacancy-to-nanohole continuous growth on GO under cyclic oxidation and reduction at 1000 K. (a–c) Images of the models after (a) the reduction-based pretreatment, (b) oxidation plus second-round reduction, and (c) second oxidation plus third-round reduction. (d) The number of the carbon atoms in graphitic rings (orange curve) and overall atoms (functional groups and carbon atoms) (black curve) changing with respect to the simulation time. The inset image is the original GO flake.

The MD results are analyzed in Figure 4. After the first run of thermal annealing at 1000 K for pretreatment (Figure 4a), several vacancy defects are formed on the graphene basal plane and stabilizes within a period of simulation time. Then, the oxidation and the second-round annealing-based reduction are implemented (Figure 4b). The atomic vacancy on the left side of the graphene model is obviously enlarged into a nanohole. In comparison, no oxidation takes place on the right region of the graphene model (Figure 4b). No change in size of this vacancy indicates that oxidation is necessary for the continuous growth of the in-plane holes. This can be further confirmed by repeating the oxidation and annealing process for another round in Figure 4c. To quantify the removal of carbon atoms from graphitic rings, the number of sp^2 carbon atoms (orange curve) and overall atoms (carbon atoms plus additional functional groups) (black curve) as functions of simulation time are plotted in Figure 4d. As observed, both the 1st and 2nd oxidation processes increase the overall atom number in the system in Figure 4d, which is due to the addition of extra functional groups. However, the number of sp^2 carbon atoms decreases after each oxidation, confirming that the restored functional groups are reactive and can remove carbon atoms from graphene basal plane when they are later reduced. This result also indicates that at a relatively low temperature (1000 K), though it cannot create large in-plane nanoholes simply through reduction as demonstrated in Figure 2, the H_2O_2 oxidation can still considerably promote the growth of vacancies-to-nanoholes.

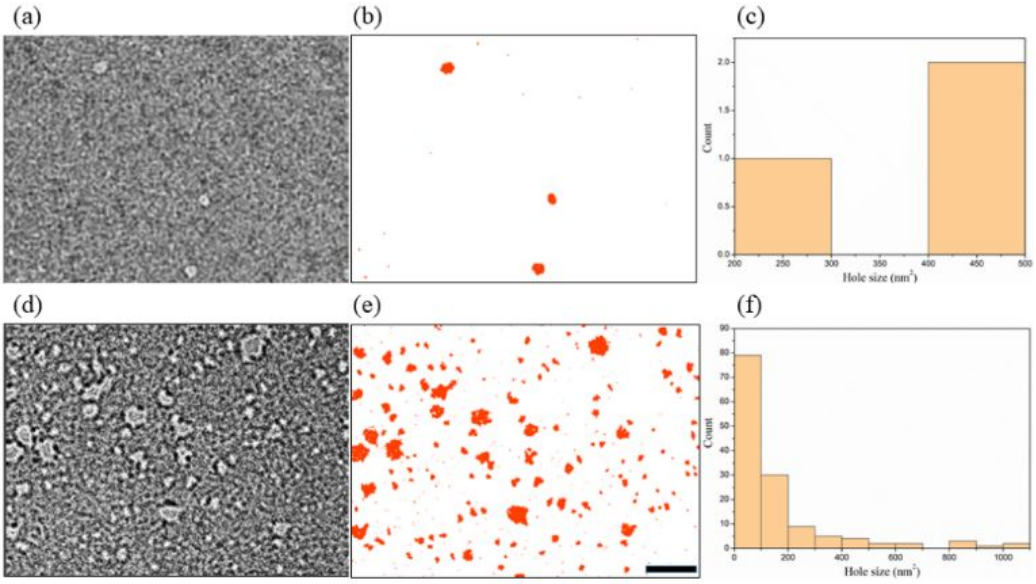

Fig. 5 TEM images and corresponding hole distribution histograms of holey GO sheets obtained w/wo pretreatment process (under the same etching process), showing the effects of preformed vacancy defects on the formation and growth of in-plane nanoholes: (a) without pretreatment; (d) pretreated by microwave heating the GO solution for 360 s. Scale bar, 100 nm.

Table 2 Hole distribution of holey GO sheets obtained w/wo pretreatment process.

Treatment	Population	Average size (nm²)	Total area (nm²)	Area percentage
No pretreatment	3	368	1105	0.36%
360s pretreatment	137	161	22049	7.24%

In summary, the encouraging simulation results above suggest that the vacancy defects generated by reduction-based pretreatment play a critical role in the holey graphene manufacturing, especially with H_2O_2 as the etchant. In other words, after defects are generated during pretreatment, the edge-site carbon atoms tend to become chemically active and react with etchant more efficiently. These findings will shed light on practical experiments, implying that a defect-forming pretreatment may be able to significantly enhance the etching efficiency, and thereby lower the reaction temperature, shorten the reaction time, and minimize the usage of aggressive chemical etchants, etc.

To verify the simulations above and further study the impacts of the pretreatment-generating vacancy defects, we conducted holey graphene manufacturing experiments using H_2O_2 as the chemical etchant. Specifically, two batches of holey GO sheets are prepared under different pretreatment conditions. The first batch is obtained by directly heating the mixture of the GO solution and H_2O_2 without pretreatment. The second batch is first pretreated by microwave heating the GO solution for 360 s at 50 W and then etched by H_2O_2 under the same condition to the first batch. The microwave heating pretreatment is selected to achieve the partial reduction of GO according to prior studies[21]. We believe the density of vacancy defects on GO sheets can vary upon w/wo pretreatment as demonstrated in our previous publication[19], so the growth of in-plane nanoholes is different for these two batches of resulted holey GO sheets.

Microscopic observations of the holey GO sheets collected are shown in Figure 5. As shown, the holey GO sheet without pretreatment (Figure 5a) has far less in-plane holes than the one with the microwave heating pretreatment (Figure 5d) in the regions with a same area. To better recognize the nanoholes formed on the GO sheets, the ImageJ software was used to recognize the holes and mark them into red color as shown in Figures 5b and 5e. In comparison, both the density and size of the holes increase after introducing the pretreatment. Figures 5c and 5f further analyze the density and size of the etched nanoholes. Without the partial reduction-based pretreatment (Figure 5c), only 3 observed holes are formed in size averagely ~ 368 nm^2, and the total holey area is 1105 nm^2 taking around 0.36% of the observed GO sheet (Table 2). The formation of these holes might be attributed to the fact that etching reactions happen on the pre-existing vacancy defects, which were induced in the original exfoliation process. On the other hand, with the pretreatment (Figure 5f), as many as 137 holes are formed, much more than the case without pretreatment. The size of the holes varies from ~50 to ~1050 nm^2, averagely 161 nm^2 due to a large number of small holes formed. The total holey area is 22049 nm^2, occupying around 7.24% of the GO sheet observed. Given the etching reaction time (as detailed in the experimental section) utilized herein is several minutes, which is much shorter than time periods reported in the prior reports[6], we can conclude that the pretreatment process must have generated a large number of vacancy defects that subsequently grow into large nanoholes. This agrees well with our simulation results above, as well as previous experimental studies demonstrating that partial reductions of GO lead to vacancy defects. In addition, the interconnection of the holes

could take place during long-time etching as seen in Figure 5d, implying hole growth and mergence with each other. Our experimental results verify that, with pretreatment-generating vacancy defects, the holey graphene manufacturing can be significantly promoted even using mild etchants like H_2O_2.

At last, we need to point out that, the GO we used in this experiment study are prepared by Hummer's method (see section 3.3) and are very likely to contain a few metal impurities. These impurities might have catalytic effects on the etching process. However, this will not change our conclusion. Because even if there are metal impurities, the hole formation is not adequate without pretreatment.

3 Method

3.1 DFT calculations

All the density functional theory (DFT) calculations are performed using the Vienna *Ab-initio* Simulation Package[22]. The maximum kinetic energy of the planewaves modeling the electron wavefunctions is set to 500 eV. The Perdew-Burke-Ernzerhof functional[23] is used for treating electron-electron exchange-correlation interactions. We also adopt the standard version of potential datasets that are created by the projector augmented-wave method[24, 25] for approximating the electron-nuclei interactions. A sufficiently large vacuum spacing of 18.0 Å in the cross-plane direction is applied to all the simulation supercells to avoid image interactions. For the *k*-point sampling, we use a single Γ point, which is sufficient because large supercells are used in our DFT calculations. We optimize the atomic configurations with a force threshold of 0.01 eV/Å.

3.2 MD simulations

MD simulations are performed using the LAMMPS[26] package with the reactive force-field (ReaxFF) describing the bond association/disassociation process during the thermal annealing of GO sheets. The oxidation of GO sheets is controlled at around 20%. Structural optimization with ReaxFF was performed at room temperature. A Berendsen thermostat with a damping parameter of 100 time-steps was used to control the system temperature. Periodic boundary conditions are applied in the x and y directions with a 10 nm vacuum space in the z direction. The time step size is 0.05 fs. Molecular by-products released from the GO sheet were removed periodically every 10 fs to mimic the experimental reduction environment against vacuum. The supercell was first gradually heated from 300 K to 1000 K over a time span of 325 fs, then annealed at 1000 K for around 5 ps, and subsequently quenched to 300 K over a time span of 1 ps. Finally, the supercell was further annealed at 300 K and zero pressure for 3 ps to ensure complete equilibration of the structure. For the second and third thermal annealing process, the hydroxyl and epoxy functional groups are only added at the defects edge generated in the previous step while keeping the same oxidation level. The thermal annealing process is repeated.

3.3 Experiment

The GO aqueous solution is prepared from graphite flakes (50+ mesh, Sigma-Aldrich) by an improved Hummer's method[27]. Then 3 mg/mL GO solution (3 mL) is added into a glass vial with a PTFE cap and processed (pretreatment) in a microwave reactor (Anton Paar Monowave 400, 2.45 GHz) at a constant power of 50 W for 360 s, while stirred at a speed of 600 rpm. After cooling, 1 mL H_2O_2 (30%) is added into the vial, then repeat the same microwave process (etching). To confirm the existing of holes, the GO sheets are characterized by a TEM (FEI Titan, 300/80) at 300 kV.

Conclusions

The fundamental mechanisms involved in holey graphene fabrication via chemical etching is investigated. Research results indicate that the formation of nanoholes in graphene basal planes is achieved by a three-stage procedure of reduction-oxidation-reduction, as illustrated in Figure 1. In specific, the vacancy defects on graphene sheets formed by a partial reduction-based pretreatment are preferentially oxidized by H_2O_2. After the oxidation, the carbon chains around the defects are anchored by various reactive functional groups, which are then removed along with the neighboring carbon atoms due to reduction reactions. This three-stage procedure facilitates the growth of atomic vacancies into large nanoholes on graphene basal planes. It is also demonstrated that a defect-forming pretreatment process can significantly promote the etching reactions for holey graphene manufacturing.

Author contributions

This work was devised by QN, DW and RD. KB and DW performed the experimental measurements. KB performed the image processing for statistical calculations of fabricated structures. RD conducted computational simulations with assistance from LL and HZ. All authors co-wrote the manuscript.

Conflicts of interest

There are no conflicts to declare.

Acknowledgements

This study is partially supported by NSF grants CMMI-1826392, CMMI-1825576, and CMMI-1825608. We acknowledge the use of facilities within the Eyring Materials Center at Arizona State University supported in part by NNCI-ECCS-1542160.

References

1. Z. Chen, X. An, L. Dai and Y. Xu, *Nano Energy*, 2020, 104762.
2. R. Raccichini, A. Varzi, S. Passerini and B. Scrosati, *Nature Materials*, 2015, **14**, 271.
3. Y. Bai, X. Yang, Y. He, J. Zhang, L. Kang, H. Xu, F. Shi, Z. Lei and Z.-H. Liu, *Electrochimica Acta*, 2016, **187**, 543-551.
4. Y. Xu, Z. Lin, X. Zhong, X. Huang, N. O. Weiss, Y. Huang and X. Duan, *Nat Commun*, 2014, **5**, 4554.

5. X. Zhao, C. M. Hayner, M. C. Kung and H. H. Kung, *ACS Nano*, 2011, **5**, 8739-8749.
6. Y. Xu, C.-Y. Chen, Z. Zhao, Z. Lin, C. Lee, X. Xu, C. Wang, Y. Huang, M. I. Shakir and X. Duan, *Nano Letters*, 2015, **15**, 4605-4610.
7. P. Xu, Q. Gao, L. Ma, Z. Li, H. Zhang, H. Xiao, X. Liang, T. Zhang, X. Tian and C. Liu, *Carbon*, 2019, **149**, 452-461.
8. J. Zhao, Y.-Z. Zhang, F. Zhang, H. Liang, F. Ming, H. N. Alshareef and Z. Gao, *Advanced Energy Materials*, 2019, **9**, 1803215.
9. M. Zhao, *Applied Sciences*, 2018, **8**, 1303.
10. L. Liu, S. Ryu, M. R. Tomasik, E. Stolyarova, N. Jung, M. S. Hybertsen, M. L. Steigerwald, L. E. Brus and G. W. Flynn, *Nano Letters*, 2008, **8**, 1965-1970.
11. Y. Xu, Z. Lin, X. Zhong, X. Huang, N. O. Weiss, Y. Huang and X. Duan, *Nature Communications*, 2014, **5**.
12. X. Dong, N. Hu, L. Wei, Y. Su, H. Wei, L. Yao, X. Li and Y. Zhang, *Journal of Materials Chemistry A*, 2016, **4**, 9739-9743.
13. J. G. Radich and P. V. Kamat, *ACS Nano*, 2013, **7**, 5546-5557.
14. R. S. Ribeiro, A. M. T. Silva, J. L. Figueiredo, J. L. Faria and H. T. Gomes, *Carbon*, 2013, **62**, 97-108.
15. W. Xing, G. Lalwani, I. Rusakova and B. Sitharaman, *Particle & Particle Systems Characterization*, 2014, **31**, 745-750.
16. D. R. Dreyer, S. Park, C. W. Bielawski and R. S. Ruoff, *Chemical Society Reviews*, 2010, **39**, 228-240.
17. W. Cai, R. D. Piner, F. J. Stadermann, S. Park, M. A. Shaibat, Y. Ishii, D. Yang, A. Velamakanni, S. J. An, M. Stoller, J. An, D. Chen and R. S. Ruoff, 2008, **321**, 1815-1817.
18. M. J. Yoo and H. B. Park, *Carbon*, 2019, **141**, 515-522.
19. D. Wang, R. Dai, X. Zhang, L. Liu, H. Zhuang, Y. Lu, Y. Wang, Y. Liao and Q. Nian, *Carbon*, 2020, **161**, 880-891.
20. A. Shen, Y. Zou, Q. Wang, R. A. W. Dryfe, X. Huang, S. Dou, L. Dai and S. Wang, *Angewandte Chemie*, 2014, **126**, 10980-10984.
21. X. Xie, Y. Zhou and K. Huang, *Frontiers in Chemistry*, 2019, **7**.
22. G. Kresse and J. Furthmüller, *Computational Materials Science*, 1996, **6**, 15-50.
23. J. P. Perdew, K. Burke and M. Ernzerhof, *Physical Review Letters*, 1996, **77**, 3865-3868.
24. G. Kresse and D. Joubert, *Physical Review B*, 1999, **59**, 1758-1775.
25. P. E. Blöchl, *Physical Review B*, 1994, **50**, 17953-17979.
26. B. FrantzDale, S. J. Plimpton and M. S. Shephard, *Engineering with Computers*, 2010, **26**, 205-211.
27. D. C. Marcano, D. V. Kosynkin, J. M. Berlin, A. Sinitskii, Z. Sun, A. Slesarev, L. B. Alemany, W. Lu and J. M. Tour, *ACS Nano*, 2010, **4**, 4806-4814.